

On the geometry of broad emission region in quasars

R. Decarli,^{1*} M. Labita,¹ A. Treves,¹ R. Falomo²

¹ *Università degli Studi dell'Insubria, via Valleggio 11, 22100 Como, Italy*

² *INAF - Osservatorio Astronomico di Padova, Vicolo dell'Osservatorio 5, 35122, Padova, Italy*

2 February 2022

ABSTRACT

We study the geometry of the $H\beta$ broad emission region by comparing the M_{BH} values derived from $H\beta$ through the virial relation with those obtained from the host galaxy luminosity in a sample of 36 low redshift ($z \sim 0.3$) quasars. This comparison lets us infer the geometrical factor f needed to de-project the line-of-sight velocity component of the emitting gas. The wide range of f values we found, together with the strong dependence of f on the observed line width, suggests that a disc-like model for the broad line region is preferable to an isotropic model, both for radio loud and radio quiet quasars. We examined similar observations of the C IV line and found no correlation in the width of the two lines. Our results indicate that an inflated disc broad line region, in which the Carbon line is emitted in a flat disc while $H\beta$ is produced in a geometrically thick region, can account for the observed differences in the width and shape of the two emission lines.

Key words: galaxies: active - galaxies: nuclei - quasars: general - quasars: emission lines

1 INTRODUCTION

Super-massive black holes (BHs) are found in virtually all massive spheroids (Kormendy & Richstone 1995). In the Local Universe BH mass measurements can be performed through their imprint on the stellar kinematics (see Ferrarese 2006 and references therein). The masses of the BHs are correlated with some large scale properties of their host galaxies (Ferrarese & Merritt 2000; Gebhardt et al. 2000; Magorrian et al. 1998; Marconi & Hunt 2003; Graham & Driver 2007). The reader is referred to Graham (2007) for an up-to-date review on this topic, and to King (2005) and references therein for interpretative models of the scaling relations.

In Type-1 AGNs the line emission from the gas inside the BH radius of influence is observed. If non-gravitational motions are neglected, the cloud velocity at a given radius is fixed by the BH mass M_{BH} . Emission lines are Doppler broadened according to the gas motions. A simple, isotropic model of the broad line region (BLR) is usually adopted (e.g., Salvander et al. 2007 and the references therein); McLure & Dunlop (2002), Dunlop et al. (2003) and Laor et al. (2006) found that a disc model is preferable, and Decarli et al. (2008) proved that inclination may explain some peculiar characteristics of the so-called Narrow Line Type-1 AGNs. On the other hand, some authors questioned

the underlying virial assumption (Bottorff et al. 1997), at least for some broad emission lines (e.g., Baskin & Laor 2005). McLure & Dunlop (2001) and Dunlop et al. (2003), and, more recently, a number of reverberation mapping campaigns (e.g., Metzroth Onken & Peterson 2006; Bentz et al. 2007; Sergeev et al. 2007) found rough agreement between the virial estimate of the BH mass from $H\beta$ width and the one based on the host galaxy luminosities, but the observed dispersions are significant. If the scatter is due to the assumed gas dynamical model, constrains on the BLR geometry can be inferred. Onken et al. (2004) compared the virial estimates of M_{BH} in few, well studied nearby AGNs with the stellar velocity dispersion of their host galaxies. The large offset observed with respect to the relation observed in inactive galaxies suggested that an isotropic geometry is not successful, but they could not put a better constrain on the gas dynamics due to the large uncertainties and the poor statistics. In radio loud quasars (RLQs), the width of the broad lines is roughly correlated to the core-to-lobe power ratio index, $R_{\text{c-1}}$ (e.g., Wills & Browne 1986; Brotherton 1996; Vestergaard Wilkes & Barthel 2000). This dependence is usually interpreted in terms of a flat BLR, given that $R_{\text{c-1}}$ is related to the inclination angle of the jet axis with respect to the line of sight. Whether a flat BLR model can be valid also for radio quiet quasars (RQQs) is still unclear.

$H\beta$ is the best studied emission line for low-redshift objects, while $\text{Mg II}_{\lambda 2798}$ and $\text{C IV}_{\lambda 1549}$ are often chosen for

* roberto.decarli@mib.infn.it

Table 1. Sample properties and imaging data from literature. (1), (4)-(6): object name, redshift, radio loudness (‘Q’=radio quiet; ‘L’=radio loud) and V apparent magnitude from Veron-Cetty & Veron (2006). (2)-(3): target coordinates from NED. (7): host galaxy absolute R magnitude corrected as described in section 3.1. (8): estimated M_{BH} using equation 1.

Object name (1)	R.A. (J2000.0) (2)	Decl. (J2000.0) (3)	z (4)	Radio (5)	V [mag] (6)	M_R [mag] (7)	$\log M_{\text{BH}}$ [M_{\odot}] (8)
0054+144	00 57 09.9	+14 46 10	0.171	Q	15.70	-22.48	8.6
0100+0205	01 03 13.0	+02 21 10	0.393	Q	17.51	-22.00	8.4
0110+297	01 13 24.2	+29 58 15	0.363	L	17.00	-22.85	8.8
0133+207	01 36 24.4	+20 57 27	0.425	L	18.10	-22.69	8.7
3C48	01 37 41.3	+33 09 35	0.367	L	16.20	-24.76	9.8
0204+292	02 07 02.2	+29 30 46	0.109	Q	16.80	-22.80	8.8
0244+194	02 47 40.8	+19 40 58	0.176	Q	16.66	-22.29	8.5
0624+6907	06 30 02.5	+69 05 04	0.370	Q	14.20	-24.53	9.6
07546+3928	07 58 00.0	+39 20 29	0.096	Q	14.36	-24.08	9.4
US1867	08 53 34.2	+43 49 02	0.513	Q	16.40	-23.39	9.1
0903+169	09 06 31.9	+16 46 11	0.412	L	18.27	-22.76	8.8
0923+201	09 25 54.7	+19 54 05	0.190	Q	15.80	-22.15	8.4
0944.1+1333	09 46 52.0	+13 20 26	0.131	Q	16.05	-23.23	9.0
0953+415	09 56 52.4	+41 15 22	0.234	Q	15.30	-22.24	8.4
1001+291	10 04 02.5	+28 55 35	0.330	Q	15.50	-23.42	9.1
1004+130	10 07 26.1	+12 48 56	0.240	L	15.20	-23.10	8.9
1058+110	11 00 47.8	+10 46 13	0.423	L	17.10	-22.46	8.6
1100+772	11 04 13.7	+76 58 58	0.315	L	15.72	-23.55	9.1
1150+497	11 53 24.4	+49 31 09	0.334	L	17.10	-23.66	9.2
1202+281	12 04 42.1	+27 54 11	0.165	Q	15.60	-22.40	8.6
1216+069	12 19 20.9	+06 38 38	0.331	Q	15.65	-22.29	8.5
Mrk0205	12 21 44.0	+75 18 38	0.071	Q	15.24	-22.63	8.7
1222+125	12 25 12.9	+12 18 36	0.411	L	17.86	-23.22	9.0
1230+097	12 33 25.8	+09 31 23	0.415	Q	16.15	-23.89	9.3
1307+085	13 09 47.0	+08 19 49	0.155	Q	15.10	-21.89	8.3
1309+355	13 12 17.8	+35 15 21	0.184	L	15.64	-23.29	9.0
1402+436	14 04 38.8	+43 27 07	0.323	Q	15.62	-22.96	8.8
1425+267	14 27 35.5	+26 32 14	0.366	L	15.68	-23.04	8.9
1444+407	14 46 45.9	+40 35 06	0.267	Q	15.70	-22.66	8.7
1512+37	15 14 43.0	+36 50 50	0.371	L	16.27	-23.09	8.9
3C323.1	15 47 43.5	+20 52 17	0.266	L	16.70	-23.06	8.9
1549+203	15 52 02.3	+20 14 02	0.250	Q	16.40	-21.86	8.3
1635+119	16 37 46.5	+11 49 50	0.146	Q	16.50	-22.40	8.6
3C351	17 04 41.4	+60 44 31	0.372	L	15.28	-23.55	9.1
1821+643	18 21 57.3	+64 20 36	0.297	Q	14.10	-24.44	9.6
2141+175	21 43 35.5	+17 43 49	0.213	L	15.73	-23.13	8.9
2201+315	22 03 15.0	+31 45 38	0.295	L	15.58	-24.28	9.5
2247+140	22 50 25.3	+14 19 52	0.235	L	16.93	-23.11	8.9

higher redshift (e.g. McLure & Jarvis 2002, Peterson et al. 2004, Kaspi et al. 2005 and 2007, Peng et al. 2006), since they fall in the optical range for $z \gtrsim 0.4$ and $z \gtrsim 1.6$ respectively. Mg II and $\text{H}\beta$ widths are well correlated (Salviander et al. 2007), while C IV line shows systematic deviances from the $\text{H}\beta$ values (Baskin & Laor 2005, Vestergaard & Peterson 2006). Labita et al. (2006) studied M_{BH} derived from C IV width as a function of a L_{bulge} -based M_{BH} for a sample of low-redshift quasars. They found a significantly better correlation than that reported by McLure & Dunlop (2001) for $\text{H}\beta$ data.

In this paper we study the BLR geometry and gas dynamics by comparing the M_{BH} values derived from $\text{H}\beta$ broad emission with those obtained from the host galaxy luminosity in a sample of 36 low redshift ($z \sim 0.3$) quasars. The sample is selected in order to provide similar numbers of RLQs and RQQs, so that conclusions on the geometry of the BLR can be drawn for both classes. Comparing our results with those of Labita et al. (2006), based on C IV line, we sketch a picture of the dynamics of the gas around the BH. Note that since the dynamical model of the BLR is assumed to be independent of redshift, we also test the evolution of the BH–host galaxy relations.

We define our sample in section 2. Data sources are summarized in section 3. Data analysis is described in section 4. We then discuss our results (section 5). The sketch of the broad line region dynamics is presented in section 6. Throughout the paper we adopt a concordance cosmology with $H_0 = 72 \text{ km/s/Mpc}$, $\Omega_m = 0.3$ and $\Omega_\Lambda = 0.7$. We converted the results of other authors to this cosmology when adopting their relations and data.

2 THE SAMPLE

We selected all quasars in the Veron-Cetty & Veron (2006) catalogue that have been imaged by *HST*-WFPC2 (exposure time $> 1000 \text{ s}$). The host galaxies are required to be elliptical, and therefore the bulge component practically coincides with the whole galaxy. We considered all the quasars with $z < 0.6$, so that the $\text{H}\beta_{\lambda 4861} - [\text{O III}]_{\lambda\lambda 4959,5007}$ lines are present in the optical spectra. For their observability from the Northern hemisphere, we selected only objects with $\delta > 0^\circ$. The entire sample thus consists of 53 targets. 12 of them have available spectra in the Sloan Digital Sky Survey (SDSS; see section 3.2). Other 32 spectra were taken on purpose at the Asiago Observatory (see section 3.2), including

6 targets already observed by the SDSS. Two observed targets were then excluded from our analysis: 0903+169 (RQQ) because of the low signal to noise ratio in the available spectrum, and 0923+201 (RLQ) because of the peculiar, composite profile of its broad lines, possibly due to the interaction with a nearby galaxy (see McLeod & Rieke 1994; Bennert et al. 2007). Thus ~ 70 per cent of the sample was covered, including 16 RLQs and 20 RQQs. Table 1 summarizes the main properties of the objects in our sample.

3 DATA SOURCES

3.1 Host galaxy magnitudes and M_{BH}

The host galaxy apparent R magnitudes were taken from the literature (Hooper et al. 1997; Boyce et al. 1998; Kirhakos et al. 1999; Pagani et al. 2003; Dunlop et al. 2003; Labita et al. 2006) or converted from published V or $F702W$ luminosities (Bahcall et al. 1997; Hamilton et al. 2002; Floyd et al. 2004). Corrections for galactic extinction are from Schlegel et al. (1998). To perform colour and k -correction transformations we adopted an elliptical galaxy template (Mannucci et al. 2001), assuming that the host galaxies are dominated by old stellar population. The k -correction for an elliptical galaxy at $z = 0.3$ observed in the R -band is 0.3 mag. The passive evolution of the host galaxies follows Bressan, Chiosi & Fagotto (1994), as discussed in Labita et al. (2006). Typical corrections for the passive evolution are ~ -0.3 mag. The resulting R -band absolute magnitudes of the host galaxies are given in table 1.

We use the relationship obtained by Bettoni et al. (2003), corrected for the chosen cosmology, in order to estimate M_{BH} from the host galaxy luminosity:

$$\log M_{\text{BH}} = -0.50M_R - 2.60 \quad (1)$$

where M_R is the absolute magnitude of the bulge component of the host galaxy. The rms of this fit is 0.39. Table 1 also lists the resulting M_{BH} values.

3.2 Spectroscopic observations

32 optical spectra were taken with the 1.82m Cima Ekar telescope at the Asiago Observatory. The Asiago Faint Object Spectrograph Camera was mounted in longslit spectroscopy configuration with grisms n. 4, 7 and 8, yielding spectral resolutions of $R \sim 300$, 555 and 900 (2.10" slit) in the spectral range 3500–7800 Å, 4300–6500 Å and 6200–8050 Å respectively ($\Delta\lambda/\text{pxl} = 4.24$, 2.10 and 1.78 Å/pxl). At $\lambda \approx 5000$ Å the spectral instrumental resolutions are ~ 17 , 9.1 and 5.5 Å, tight enough to distinguish prominent H β narrow emission from the broad one.

The standard IRAF procedure was adopted in the data reduction. The **ccdred** package was employed to perform bias subtraction, flat field correction, image alignment and combination. Cosmic rays were eliminated by combining 3 or more exposures of the same objects, and applying **crreject** algorithm while averaging. When only one or two bidimensional spectra were available, we applied **cosmicrays** task in the **crutils** package. In order to prevent the task from altering the narrow component of emission lines, we masked the central region of our bidimensional spectra. The spectra

Table 2. Sample objects spectroscopically observed at the Asiago Observatory. Redshifts and V magnitudes are taken from Veron-Cetty & Veron (2006). In the “Available spectra” column, Ax=Asiago + grism n.x; S=SDSS; H=*HST*-FOS archive data analyzed in Labita et al. (2006). Seeing is measured on corollary R -band imaging. These images were not available for objects 0100+020 and 3C48.

Object name (1)	z (2)	V [mag] (3)	Available spectra (4)	Date (5)	Seeing [arcsec] (6)
0054+144	0.171	15.70	A4,S	13/09/06	1.4
0100+020	0.393	16.39	A4,H	18/09/07	n/a
0110+297	0.363	17.00	A4	09/12/05	2.1
0133+207	0.425	18.10	A4,H	27/11/06	2.0
3C48	0.367	16.20	A4	11/12/05	n/a
0204+2916	0.109	16.80	A4	15/10/06	1.7
0244+194	0.176	16.66	A4	16/10/06	1.7
0624+6907	0.370	14.20	A4,H	27/10/06	2.6
07546+3928	0.096	14.36	A4	24/12/05	1.9
US1867	0.513	16.40	A4,S,H	27/11/06	1.3
0944.1+1333	0.131	16.05	A4	25/04/06	2.4
0953+415	0.234	15.30	A4	07/02/06	3.1
1001+291	0.330	15.50	A4	19/02/06	2.4
1004+130	0.240	15.20	A4,S	07/03/06	2.2
1058+110	0.423	17.10	A4,S	26/04/06	2.0
1100+772	0.315	15.72	A4	08/03/06	2.7
1202+281	0.165	15.60	A4,H	20/02/06	2.3
1216+069	0.331	15.65	A8,H	12/04/07	1.9
Mrk0205	0.071	15.24	A7,H	11/04/07	1.6
1307+085	0.155	15.10	A7,H	24/04/07	1.6
1309+355	0.184	15.64	A4,H	20/02/06	2.4
1402+436	0.323	15.62	A4,S	07/03/06	3.6
1425+267	0.366	15.68	A4,H	20/02/06	2.9
3C323.1	0.266	16.70	A7,H	24/04/07	1.4
1549+203	0.250	16.40	A4	23/04/06	2.0
1635+119	0.146	16.50	A4	31/05/06	2.8
1821+643	0.297	14.10	A4,H	15/12/06	2.1
2141+175	0.213	15.73	A4,H	15/12/06	1.9
2201+315	0.295	15.58	A4,H	15/12/06	1.5
2247+140	0.235	16.93	A4,S,H	12/09/06	1.5

extraction, the background subtraction and the calibrations both in wavelength and in flux were performed with **doslit** task in **kpnoslit** package, using a Hg-Cd and Ne lamps and spectrophotometric standard stars as reference. Wavelength calibration residuals are around 0.17 Å (sub-pixel), thus implying a negligible (< 1 per cent) error on redshift estimates. Absolute calibration of spectra was corrected through the photometry of field stars, by comparing corollary imaging with Johnson’s R and V filters to the magnitudes published in the U.S. Naval Observatory catalogue. The uncertainty in the flux calibration is 0.1 mag. Galactic extinction was accounted for according to Schlegel, et al. (1998), assuming $R_V = 3.1$.

Table 2 summarizes the observed targets.

The SDSS Data Release 5 (Adelman-McCarthy, et al., 2007) provides spectra for 12 quasars in our sample. SDSS spectra have $R \sim 2000$ and a spectral range between 3800 and 9000 Å. Uncertainties on wavelength calibration amount to 0.05 Å, while flux calibration formal errors account to 5 per cent. We re-observed six of these objects (0054+144, US1867, 1004+130, 1058+110, 1402+436, 2247+140) in order to perform a comparison. Both the specific fluxes at 5100 Å and the H β broad line widths are in good agreement. Due to their better spectral resolution, we will consider only the SDSS spectra of these objects in our analysis.

4 THE VIRIAL DETERMINATION OF M_{BH}

In the virial assumption, if the velocity v of a particle orbiting at a certain radius R around the BH is known, the mass of the BH is simply:

$$M_{\text{BH}} = \frac{Rv^2}{G} \quad (2)$$

In Type-1 AGNs expression (2) can be evaluated at the characteristic radius of the BLR, $R = R_{\text{BLR}}$, which can be measured almost directly with the reverberation mapping technique (Blandford & McKee 1982). Kaspi et al. (2000) found that the nuclear monochromatic luminosity, λL_λ , is correlated with R_{BLR} by $\lambda L_\lambda \propto R_{\text{BLR}}^\gamma$, with γ depending on the considered emission line. The broad line width is used to estimate $v_{\text{BLR}} = v(R_{\text{BLR}})$. According to the adopted dynamical model,

$$v_{\text{BLR}} = f \cdot \text{FWHM} \quad (3)$$

where f is a geometrical factor¹ and the FWHM is expressed in velocity units. If the gas moves isotropically, a gaussian line shape is observed, with $f \approx \sqrt{3}/2$. If a rotational component is present, an axial symmetry is introduced, and f depends on the inclination angle ϑ :

$$f = \left(2c_1 \sin \vartheta + \frac{2}{\sqrt{3}} c_2 \right)^{-1} \quad (4)$$

where ϑ is the angle between the line of sight and the rotation axis, and c_1 and c_2 are parameters accounting for the importance of the disc and isotropic components respectively. The reader is referred to McLure & Dunlop (2001), Labita et al. (2006), Collin et al. (2006) and Decarli et al. (2008) for detailed discussions on this topic. Since f value is generally unknown, one defines the Virial Product as:

$$VP = M_{\text{BH}} \cdot f^{-2} = G^{-1} R_{\text{BLR}} (\text{FWHM})^2, \quad (5)$$

corresponding to M_{BH} if f is taken unitary. Thus, an estimate of f requires measures of the monochromatic luminosity λL_λ , of the line width and independently of M_{BH} .

4.1 The monochromatic luminosity

The continuum luminosity was calculated as follows: Rest-frame spectral continua were fitted with a power-law (see figure 1). The key-point is to avoid contaminations due to various emission features, especially to broad Fe II bands. Typical rest-frame fitted regions are around 2610, 3030, 4030, 4190, 5080 Å and in the 5450-5720 Å range. The ~ 5100 Å region is generally free from contaminations and can be easily fitted. The resulting fit function was computed at 5100 Å, thus providing $\lambda F_\lambda(5100 \text{ Å})$. We corrected for the host galaxy contamination by computing the fraction of its flux within the slit, on the basis of the nucleus and host galaxy luminosities and the effective radius estimates available from the literature, and following the recipe adopted by Sbarufatti et al. (2006). The average correction is 0.06 dex.

¹ The reader should notice that different definitions for f are available in literature: Vestergaard & Peterson (2006) and Collin et al. (2006) use $M_{\text{BH}} = f \cdot G^{-1} R_{\text{BLR}} (\text{FWHM})^2$.

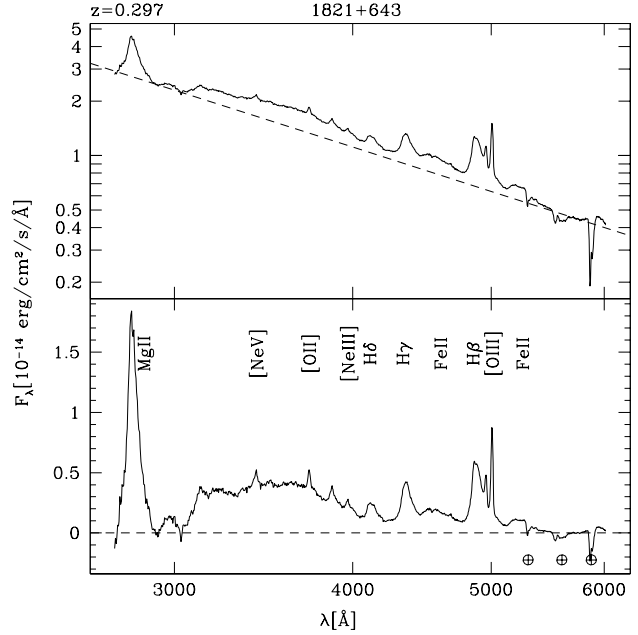


Figure 1. The rest-frame spectrum of 1821+643. The upper panel shows the observed spectrum with the fitted power-law for the continuum. The lower panel shows the residual after continuum subtraction. Main emission lines and the atmospheric absorption features are also labeled. All the spectra are available in electronic format at www.dfm.uninsubria.it/astro/caqos/index.html.

4.2 Line width measurements

The observed H β broad component is usually contaminated by other spectral features, in particular by blended Fe II multiplets, the H β narrow component and the [O III] $_{\lambda\lambda 4959,5007}$ lines.

Strong Fe II emissions are commonly detected in quasar spectra at 4400-4750 and 5150-5450 Å, and weaker blended features are found at 4800-5000 Å. A common practice to remove this contamination (e.g., Boroson & Green 1992; Marziani et al. 2003; Salvander et al. 2007; McGill et al. 2007) is to adopt the spectrum of I Zw001 as a template of the Fe II emission, due to the intensity and narrowness of the Fe II lines. Since the relative intensities of the various Fe II features may differ from a quasar to another (see, for example, table 7 in Phillips 1978), we preferred a more conservative approach: we modeled the Fe II emission as a simple power-law fitted at ~ 4750 and ~ 5100 Å, and subtracted it from the observed spectrum. The reliability of this procedure is discussed in appendix A1.

Since most of our objects have the H β red wing contaminated by [Fe VIII] $_{\lambda 4894}$, Fe II $_{\lambda\lambda 4924,5018}$ and [O III] $_{\lambda\lambda 4959,5007}$ lines, a reliable study of the broad line asymmetries is extremely hard to achieve, and is strongly dependent on the procedure adopted in removing these contaminations. We preferred to set the same peak wavelength for both the gaussian curves, thus neglecting line asymmetries. In appendix A2 we discuss how the use of a different fitting function, sensitive to the asymmetries in the line profile, does not affect the estimates of the line width in a significant way.

Table 3. Continuum luminosity parameters. (1): object name. (2): object measured redshift. (3): data set. ‘A’ refers to Asiago data, the number referring to the adopted grism; ‘S’ refers to SDSS data. (4): $\log F_\lambda(5100\text{\AA})$, computed as described in section 4.1. (5): final $\log \lambda L_\lambda$ [erg/s]. (6): computed $\log R_{\text{BLR}}$ [cm].

Object name (1)	z (2)	Data set (3)	$\log F_\lambda$ [erg/s/cm ² /Å] (4)	$\log \lambda L_\lambda$ [erg/s] (5)	$\log R_{\text{BLR}}$ [cm] (6)
0054+144	0.171	S	-14.9	44.7	17.2
0100+0205	0.393	A4	-15.6	44.9	17.3
0110+297	0.363	A4	-15.5	44.7	17.2
0133+207	0.424	A4	-15.6	44.7	17.2
3C48	0.369	A4	-14.9	45.4	17.6
0204+292	0.110	A4	-15.1	44.2	16.8
0244+194	0.174	A4	-15.1	44.7	17.2
0624+6907	0.370	A4	-14.5	46.1	18.1
07546+3928	0.096	A4	-14.2	44.7	17.2
US1867	0.515	S	-15.3	45.3	17.6
0944.1+1333	0.134	A4	-14.8	44.5	17.1
0953+415	0.235	A4	-14.8	45.6	17.8
1001+291	0.330	A4	-14.9	45.1	17.5
1004+130	0.241	S	-14.7	45.2	17.5
1058+110	0.423	S	-15.9	44.6	17.1
1100+772	0.311	A4	-14.4	45.8	17.9
1150+497	0.334	S	-15.6	44.6	17.1
1202+281	0.165	A4	-15.3	44.6	17.1
1216p069	0.331	A8	-14.7	45.6	17.8
Mrk0205	0.071	A7	-14.7	44.5	17.0
1222+125	0.412	S	-15.6	44.8	17.2
1230+097	0.416	S	-15.2	45.2	17.5
1307p085	0.155	A7	-15.0	45.3	17.6
1309+355	0.184	A4	-14.7	44.4	17.0
1402+436	0.323	S	-14.7	45.4	17.7
1425+267	0.366	A4	-15.4	45.2	17.5
1444+407	0.267	S	-14.9	45.1	17.4
1512+37	0.371	S	-15.3	45.0	17.4
3C323.1	0.266	A7	-15.2	45.2	17.5
1549+203	0.253	A4	-15.2	44.8	17.3
1635+119	0.148	A4	-15.4	42.2	15.5
3C351	0.372	S	-14.7	45.6	17.8
1821+643	0.297	A4	-14.2	46.1	18.1
2141+175	0.211	A4	-15.0	45.0	17.4
2201+315	0.295	A4	-14.9	45.4	17.7
2247+140	0.235	S	-15.3	44.6	17.1

The fit procedure was preferred to the width measurement directly applied to the observed data (without any fit; see for example Collin et al. 2006) since: 1) it is applicable also to low signal-to-noise spectra; 2) it does not require an accurate modeling of the narrow component; 3) it is reliable even in the largest tails, where contaminations by other emission or absorption features may be relevant.

We derived the FWHM and the second moment of the line, σ_{line} , from the fitted profile. Both FWHM and σ_{line} are corrected for instrumental spectral resolution. The ratio between FWHM and σ_{line} is used to study the shape of the line, as discussed in section 5.1. According to Collin et al. (2006), σ_{line} could be preferred to FWHM as a line width indicator, since it is strongly dependent on the line wings, i.e., to the kinematics of the innermost clouds. On the other hand, σ_{line} is very sensitive to contaminations and to the adopted FeII subtraction. Therefore, we will use the FWHM in the M_{BH} estimates, and consider σ_{line} only in the study of the line shape. Figure 2 offers an example of the fitting procedure, applied to 1821+643. Plots for the whole sample are available in electronic form at www.dfm.uninsubria.it/astro/caqs/index.html. Our $H\beta$ width estimates are listed in table 4. Typical uncertain-

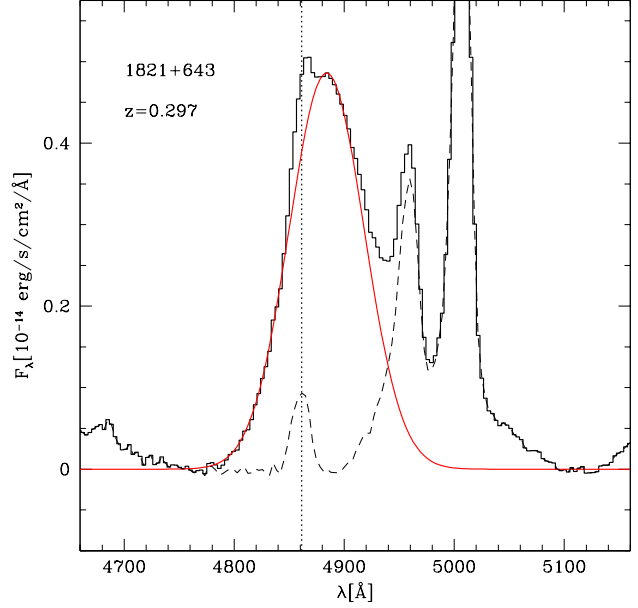


Figure 2. The rest-frame spectrum of 1821+643 in the 4660-5160 Å range. The histogram is the observed spectrum, after continuum and FeII subtraction, as described in the text. The solid, smooth line is the fitted curve. The residual after fit subtraction is plotted with a dashed line. A vertical, dotted line shows the expected $H\beta$ wavelength (4861 Å).

ties in the FWHM values due to the fit procedure are ~ 10 per cent of the line width.

5 DISCUSSION

5.1 $H\beta$ line width and shape

The mean value and rms of the $H\beta$ FWHM distribution are:

$$\langle \text{FWHM}(H\beta) \rangle_{\text{All}} = 5050 \pm 2170 \text{ km/s},$$

$$\langle \text{FWHM}(H\beta) \rangle_{\text{RLQs}} = 6100 \pm 2110 \text{ km/s},$$

$$\langle \text{FWHM}(H\beta) \rangle_{\text{RQQs}} = 4210 \pm 1870 \text{ km/s}.$$

A different distribution of FWHM is observed between RLQs and RQQs, in the sense that the former ones show, on average, wider lines than the latter. This difference may be intrinsic, the velocity of the gas in RLQs being actually larger than in RQQs, independently on the BLR geometry. Indeed, as we will notice later, a bias towards the high-mass end of the M_{BH} distribution occurs for RLQs (partially related to the Malmquist bias, since the average redshift of our sample RLQs is higher than that of RQQs). Otherwise, in the perspective of a disc-like broad line region, different average inclination angles may account for the different distributions in the FWHM values. This may be achieved assuming that, while RLQs have $0^\circ < \vartheta < 50^\circ$, the RQQs are biased towards lower inclination angles, e.g. $0^\circ < \vartheta < 40^\circ$. Such a bias has been already hypothesized by some authors (e.g., Francis et al. 2000), but its occurrence is still debated (see, for example, Kotilainen et al. 2007).

Table 4. The estimated FWHM and σ_{line} values for H β . Asiago spectra are labeled with ‘Ax’ in column (2), where x is the grism number. SDSS data are labeled with ‘S’.

Object name (1)	Data set (2)	FWHM [Å] (3)	σ_{line} [Å] (4)	FWHM [km/s] (5)	σ_{line} [km/s] (6)
0054+144	S	134	57	8220	3520
0100+0205	A4	79	35	4870	2160
0110+297	A4	100	40	6150	2440
0133+207	A4	143	53	8850	3260
3C48	A4	65	39	4010	2370
0204+292	A4	145	67	8960	4110
0244+194	A4	76	36	4680	2220
0624+6907	A4	59	32	3630	1940
07546+3928	A4	50	28	3110	1750
US1867	S	37	31	2280	1900
0944.1+1333	A4	52	30	3230	1850
0953+415	A4	58	47	3610	2890
1001+291	A4	32	26	1980	1610
1004+130	S	98	50	6010	3060
1058+110	S	121	48	7460	2950
1100+772	A4	113	58	6980	3550
1150+497	S	63	28	3870	1750
1202+281	A4	84	57	5190	3510
1216+069	A8	83	50	5110	3080
Mrk0205	A7	53	34	3270	2100
1222+125	S	122	56	7530	3430
1230+097	S	77	41	4770	2540
1307+085	A7	57	27	3520	1670
1309+355	A4	72	44	4430	2720
1402+436	S	45	33	2760	2030
1425+267	A4	131	73	8090	4530
1444+407	S	44	27	2690	1650
1512+37	S	144	52	8910	3210
3C323.1	A7	77	37	4760	2290
1549+203	A4	30	20	1880	1230
1635+119	A4	92	46	5700	2870
3C351	S	150	63	9260	3870
1821+643	A4	78	34	4820	2090
2141+175	A4	84	36	5180	2230
2201+315	A4	49	28	3020	1720
2247+140	S	52	22	3180	1330

The comparison between H β FWHM and σ_{line} illustrates some general properties of the line shape (see figure 3). A single gaussian has $\text{FWHM}/\sigma_{\text{line}} = \sqrt{8 \ln 2} \approx 2.35$. The single gaussian case (upper dashed line) represents an upper limit for FWHM. Only few H β data have $\text{FWHM} \lesssim \sigma_{\text{line}}$ (lower dashed line). Collin et al. (2006) suggested a bimodality in the FWHM vs σ_{line} relation, with a break when $\sigma_{\text{line}} \gtrsim 2000$ km/s. We argue that such a behaviour is mainly due to the fit procedure adopted by those authors: When the H β width is estimated directly on the observed spectrum, σ_{line} cannot be integrated up to infinity, because of He II $_{\lambda 4686}$, [Ar IV] $_{\lambda \lambda 4711, 4740}$ and Fe II contaminations. Integral truncation leads to underestimates of the largest line widths: For a single gaussian curve, the deviation is significant when $\sigma_{\text{line}} \gtrsim 0.5$ times the width of the truncation interval. Typically, H β can be studied only in the first 80 Å bluewards. That means, $\sigma_{\text{line}} \gtrsim 2500$ Å are underestimated. In disagreement with Collin’s results, our fit-based FWHM to σ_{line} ratio is found to be constant all over the observed values of σ_{line} . No systematic difference is reported in the FWHM/ σ_{line} ratio of RLQs and RQs.

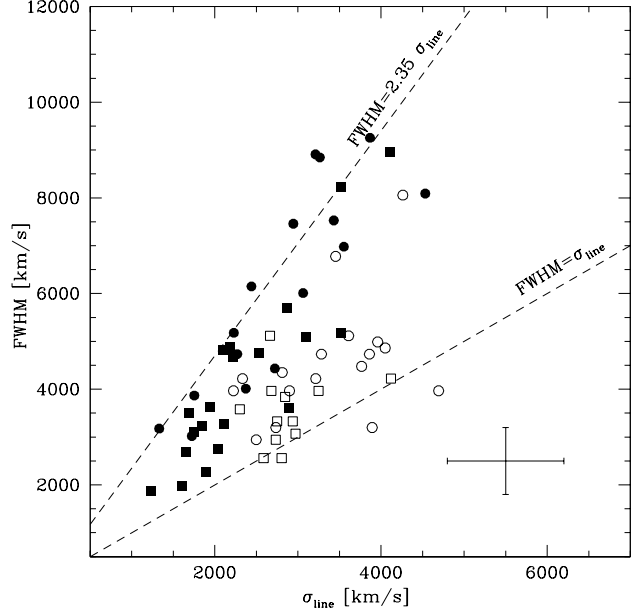


Figure 3. The FWHM as a function of σ_{line} for H β (filled symbols) and C IV (empty symbols). Circles refer to the RLQs, squares to the RQs. The dashed lines refer to $\text{FWHM} = 2.35 \sigma_{\text{line}}$ and $\text{FWHM} = \sigma_{\text{line}}$. A typical error box is also plotted. H β and C IV data clearly fill different regions of the plot. No significant difference in the FWHM/ σ_{line} ratio is observed as a function of the radio loudness.

5.2 Broad Line Region radii

Kaspi et al. (2000) found that the radius of the broad line region, as estimated by the reverberation mapping, is related to the continuum monochromatic luminosity λL_{λ} . An increasing body of measurements is now available for H β time lags (e.g. Kaspi et al. 2000, Suganuma et al. 2006, Bentz et al. 2006). Following Kaspi et al. (2005) we adopt:

$$\frac{R_{\text{BLR}}(\text{H}\beta)}{10 \text{ light-days}} = (2.00^{+0.28}_{-0.24}) \cdot \left(\frac{\lambda L_{\lambda}(5100 \text{ Å})}{10^{44} \text{ erg/s}} \right)^{0.67 \pm 0.07} \quad (6)$$

The average characteristic radius for H β is:

$$\langle \log R_{\text{BLR}}(\text{H}\beta) [\text{cm}] \rangle_{\text{All}} = 17.35 \pm 0.44$$

$$\langle \log R_{\text{BLR}}(\text{H}\beta) [\text{cm}] \rangle_{\text{RLQs}} = 17.38 \pm 0.28$$

$$\langle \log R_{\text{BLR}}(\text{H}\beta) [\text{cm}] \rangle_{\text{RQs}} = 17.33 \pm 0.55$$

where the error is the standard deviation.

5.3 Redshift dependence of the $M_{\text{BH}}-L_{\text{bulge}}$ relation

Our work is centered on the comparison between the Virial Products (equation 5) and the M_{BH} evaluated from the host galaxy luminosity. Woo et al. (2006) and Treu et al. (2007) proposed that the M_{BH} -bulge relations change significantly even at $z \approx 0.36$. On the other hand, Lauer et al. (2007) showed that such a result is probably due to a statistical bias. Owing to the steepness of the bright end of galaxy luminosity function, very high mass black holes are more com-

monly upper residuals of the M_{BH} -host luminosity, rather than being hosted by correspondingly very massive galaxies. Thus, when a luminosity cutoff is adopted (typically due to sensitivity limits, when observing at high redshift), the M_{BH} expected from $M_{\text{BH}}-L_{\text{bulge}}$ relation tends to be lower than the real one. Since the geometrical factor is supposed to be independent of redshift, we can directly test the evolution of the Bettoni relation (equation 1) checking the redshift dependence of VPs, host absolute magnitudes and their ratios. We consider here only the objects the host galaxies of which have similar luminosities, namely, the (15) objects with $-23 > M_{\text{R}} > -24$ mag, since they are roughly well distributed along the considered redshift range. While an overall slight increase in the VPs is found with redshift (possibly due to Malmquist bias), data dispersion largely exceeds the effect reported in Woo et al. (2006) and Treu et al. (2007), our objects being consistent with a no-evolution scenario. A lower scatter is observed for C IV data taken from Labita et al. (2006) (see section 5.5). Applying the same argument, no significant redshift dependence is found in the VP-to-host galaxy luminosity ratios, the probability of null correlation exceeding 30 per cent.

5.4 Spectroscopic Virial Products vs Imaging M_{BH} estimates

We are now ready to compare the Virial Products to the BH masses as estimated from the host galaxy luminosity. VPs and f values are listed in table 5. Typical uncertainties on VPs and M_{BH} are ~ 0.4 dex, due mainly to the scatter in the $R_{\text{BLR}}-\lambda L_{\lambda}$ and $M_{\text{BH}}-L_{\text{bulge}}$ relations. The comparison is shown in figure 4. Our data show no correlation: The probability of non-correlation is ~ 40 per cent, with a Spearman's rank coefficient of 0.20 and a residual standard deviation of ~ 0.50 dex. The mean value of f is 1.6 ± 1.1 . The dispersion in our data reflects the values obtained in the same way by Dunlop et al. (2003) (see their figure 13).

We study now the geometrical factor of our sample quasars separately according to radio loudness. Indeed, indications that RLQs may have flat BLRs have been already reported (in particular, the rough dependence of $R_{\text{c-1}}$ on the FWHM of $\text{H}\beta$: Wills & Browne 1986; Brotherton 1996; Vestergaard Wilkes & Barthel 2000), while not so much is known about RQQs. In RLQs, the f factor is found to be strongly dependent on the FWHM of the lines, as shown in figure 5, upper panel. We note that such a relation show significantly less dispersion than the $\text{FWHM}-R_{\text{c-1}}$ published for similar samples (e.g., see figure 4 in Brotherton 1996). Some authors proposed the existence of two different populations with different FWHM ranges and average f (Sulentic et al. 2000; Collin et al. 2006). Our data confirm this result, even if a continuous trend rather than a strict bimodality seems to be present. All the objects with $\text{FWHM} < 5000$ km/s have $f > 1$, the value of f rapidly decreasing with FWHM. According to equation 3, such a trend would be expected only if f is not fixed, given v_{BLR} . This reinforces the idea that RLQs have disc-like BLRs.

A similar picture is observed for RQQs, even if a larger dispersion is found (see, for comparison, McLure & Dunlop 2002). The occurrence of two populations is still clear: at $\text{FWHM} < 4000$ km/s all but two targets have $f > 1$, while

Table 5. Virial Products and geometrical factors for optical data. (1): object name. (2): object measured redshift. (3): Virial Products derived from $\text{H}\beta$ width and 5100 Å monochromatic luminosity. Error bars are mainly due to the intrinsic scatter in the $R_{\text{BLR}}-\lambda L_{\lambda}$ relation (~ 0.4 dex). (4): f values.

Object name (1)	z (2)	log VP ($\text{H}\beta$) [M_{\odot}] (3)	f (4)
0054+144	0.171	8.9	0.7
0100+0205	0.393	8.6	0.8
0110+297	0.363	8.6	1.1
0133+207	0.424	9.0	0.6
3C48	0.368	8.7	3.0
0204+292	0.110	8.6	1.1
0244+194	0.174	8.4	1.1
0624+6907	0.370	9.1	1.8
07546+3928	0.096	8.0	4.6
US1867	0.515	8.2	2.6
0944.1+1333	0.134	7.9	3.4
0953+415	0.235	8.8	0.7
1001+291	0.330	7.8	4.4
1004+130	0.241	9.0	0.9
1058+110	0.423	8.7	0.8
1100+772	0.311	9.5	0.6
1150+497	0.334	8.1	3.1
1202+281	0.165	8.4	1.2
1216+069	0.331	9.1	0.5
Mrk0205	0.071	8.0	2.2
1222+125	0.412	8.8	1.0
1230+097	0.416	8.8	1.7
1307+085	0.155	8.5	0.7
1309+355	0.184	8.1	2.2
1402+436	0.323	8.5	1.5
1425+267	0.366	9.2	0.7
1444+407	0.267	8.2	1.8
1512+37	0.371	9.2	0.7
3C323.1	0.266	8.8	1.1
1549+203	0.253	7.5	2.4
1635+119	0.148	6.9	0.6
3C351	0.372	9.6	0.5
1821+643	0.297	9.4	1.3
2141+175	0.211	8.7	1.3
2201+315	0.295	8.4	3.2
2247+140	0.235	8.0	2.7

only few targets with $\text{FWHM} > 4000$ km/s have $f > 1$. This rules out that the BLR is isotropic even in RQQs.

We simulated the f -FWHM relation in the hypothesis of a thin disc BLR (figure 6). We assumed a gaussian distribution of the uncertainties for FWHM, log VP and log M_{BH} , mimicking the uncertainties in the adopted fitting techniques and scaling relations. We then assumed that all the quasars have purely disc-like BLRs, with a fixed rotational velocity v_{BLR} . Fitting our data with a hyperbole (see eq. 3), we found $v_{\text{BLR}} \sim 8000$ and 6000 km/s for RLQs and RQQs respectively. The variable ϑ was let free to vary from 0 to ϑ_{max} . The angle ϑ_{max} was fixed to 40° and 50° for RLQs and RQQs respectively, in order to match the median value of the f observed distributions. The simulated values are overplotted to the measures presented in figure 5 for a comparison. We also plotted the two lines corresponding to the expected values of f if uncertainties were negligible. Both RLQs and RQQs are well described with a disc model of the BLR, with the former ones showing larger v_{BLR} than the latter ones. This difference cannot be explained in terms of a different range of ϑ , and – as we noted in section 5.1 – may be the effect of a selection bias, in the sense that the RLQs in our sample have higher average M_{BH} than RQQs.

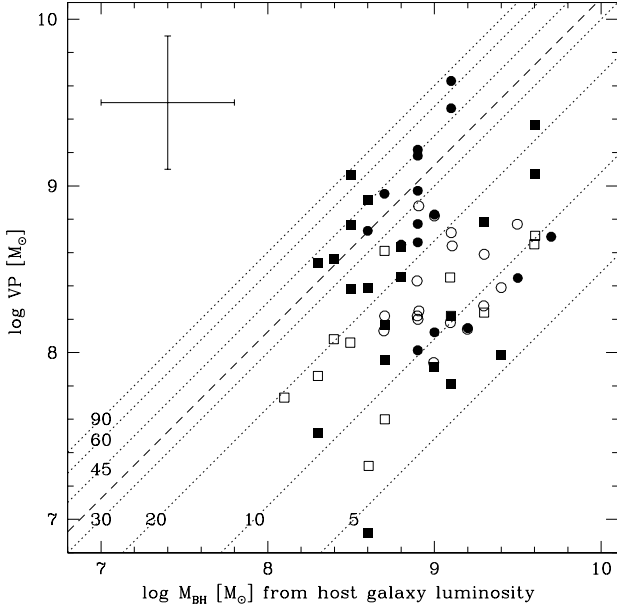


Figure 4. Comparison between spectroscopic Virial Products based on $H\beta$ and $C\text{IV}$ and M_{BH} estimates based on the bulge luminosity. Symbols are the same as in figure 3. The dashed line is the expected VP as a function of M_{BH} for an isotropic model. The values expected for a geometrically thin disc model with different inclination angles (labeled in degrees) are plotted as dotted lines.

Concerning the different FWHM distributions of RLQs and RQQs, our simulation cannot rule out a dependence on the adopted range of ϑ , as suggested by the estimates of ϑ_{max} based on the distributions of f . Extending this technique on a larger sample is needed to properly address this topic.

5.5 Comparison between $C\text{IV}$ and $H\beta$ lines

We now want to compare the $H\beta$ properties with those of the $C\text{IV}_{\lambda 1549}$ line. We will refer to the $C\text{IV}$ data in Labita et al. (2006), who used the $C\text{IV}$ line in order to measure the VPs of 29 low-redshift quasars observed with *HST*-FOS. 16 out of 29 objects in that work are also present in our sample. The average $C\text{IV}$ FWHM and its standard deviation are:

$$\langle \text{FWHM} (C\text{IV}) \rangle_{\text{All Labita sample}} = 4200 \pm 1200 \text{ km/s},$$

$$\langle \text{FWHM} (C\text{IV}) \rangle_{\text{Common sample}} = 4030 \pm 1200 \text{ km/s}.$$

$C\text{IV}$ FWHMs show smaller dispersion and a smaller mean value than $H\beta$ ones. This is remarkable: the $C\text{IV}$ line requires higher ionization potential than $H\beta$. If the virial hypothesis is valid and a simple photoionization model is assumed, $C\text{IV}$ emission should show lower radii and, accordingly to equation 2, higher velocities. In section 6 we will show how this point can be interpreted in terms of different thickness of the BLR disc at $C\text{IV}$ and $H\beta$ radii. Figure 7 shows the comparison between $C\text{IV}$ and $H\beta$ FWHMs for the objects common to both our and Labita's studies. No correlation is apparent (the probability of non-correlation

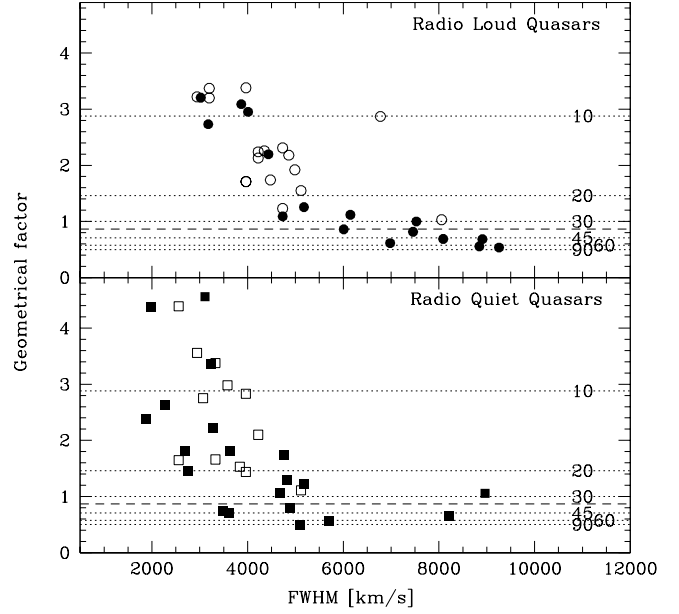


Figure 5. Comparison between the geometrical factor, f , and the FWHM for RLQs (upper panel) and RQQs (lower panel). Symbols are the same as in figure 3. The isotropic case is shown as a dashed line, while the values of f expected for a thin disc model with different inclination angles (labeled in degrees) are plotted as dotted lines.

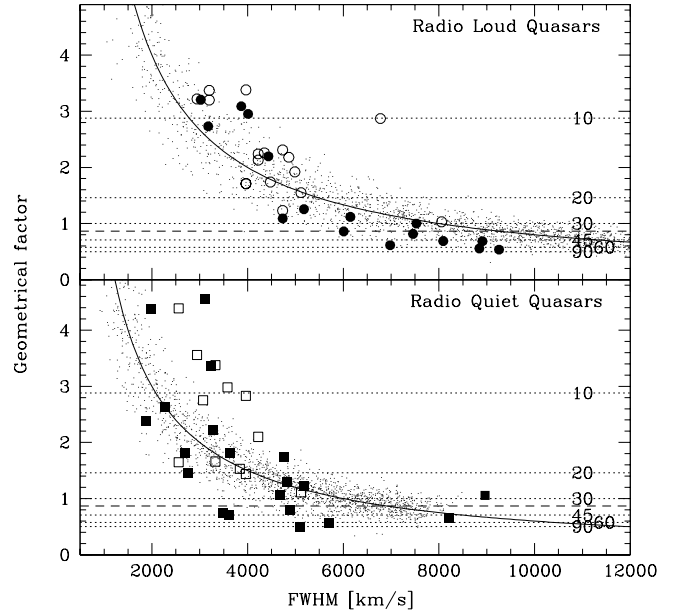


Figure 6. The f -FWHM relation for RLQs (upper panel) and RQQs (lower panel), as described in the text. Dots refer to the simulated values. The solid lines show the expected f assuming a thin-disc geometry with $v_{\text{BLR}} = 8000$ and 6000 km/s for RLQs and RQQs respectively.

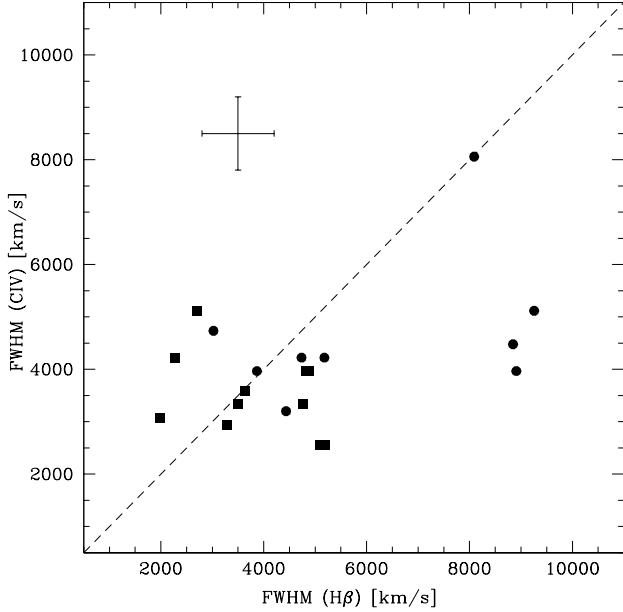


Figure 7. Comparison between $H\beta$ and C IV estimates of FWHM. Circles mark RLQs, squares refer to RQQs. A typical error box is also plotted. The dashed line is the one-to-one relation. No correlation is observed.

being up to ~ 45 per cent), as already noticed for different samples by Baskin & Laor (2005) (81 quasars) and Vestergaard & Peterson (2006) (32 quasars; see their figure 10). We argue that the FWHM values of the two lines are intrinsically different.

As in the $H\beta$ case (figure 3), we now consider the comparison between C IV FWHM and σ_{line} . Even if we sampled only a small range of σ_{line} values, the data from the two lines clearly fill different regions of the (FWHM, σ_{line}) plane. Since the fitting procedure is similar, we can rule out a systematic effect due to the width estimate algorithm. Thus, we argue that C IV and $H\beta$ broad lines have intrinsically different shapes, the C IV departing more from the isotropic (gaussian) case than $H\beta$.

The continuum monochromatic luminosity at 1350 \AA is also considered for the objects belonging to the sample of Labita et al. (2006). We use this information in order to estimate R_{BLR} for C IV data, by means of the radius-luminosity relation published by Kaspi et al. (2007):

$$\frac{R_{\text{BLR}}(\text{C IV})}{10 \text{ light-days}} = (0.24 \pm 0.06) \cdot \left(\frac{\lambda L_{\lambda}(1350 \text{ \AA})}{10^{43} \text{ erg/s}} \right)^{0.55 \pm 0.04} \quad (7)$$

This is the first available relation based on reverberation mapping studies of the C IV lines. However, it is based only on 8 sources, thus the slope and offset of the relation shall need some tuning when other data will be available. The average $R_{\text{BLR}}(\text{C IV})$ result:

$$\langle \log R_{\text{BLR}}(\text{C IV}) [\text{cm}] \rangle_{\text{All Labita sample}} = 17.19 \pm 0.31$$

$$\langle \log R_{\text{BLR}}(\text{C IV}) [\text{cm}] \rangle_{\text{Common sample}} = 17.19 \pm 0.27$$

The $R_{\text{BLR}}(\text{C IV})$ is found to be systematically (~ 1.7 times) smaller than $R_{\text{BLR}}(H\beta)$, but we warn the reader that

the scatter due to the $R_{\text{BLR}} - \lambda L_{\lambda}$ relations is severe. Values of $R_{\text{BLR}}(\text{C IV})$ smaller than $R_{\text{BLR}}(H\beta)$ are consistent with simple photoionization models: The C IV line is a higher ionization line than $H\beta$, thus it should be emitted in an inner region. Such a difference, if confirmed, should be taken into account when referring to previous works where the $R_{\text{BLR}}(H\beta)$ was used as a surrogate for $R_{\text{BLR}}(\text{C IV})$.

Following the steps traced in section 5.4, we estimate the VPs also for the C IV data. Carbon VPs are well correlated with imaging BH mass estimates (see figure 4): The probability of non-correlation is < 0.1 per cent with a Spearman's rank coefficient of 0.63 and a residual standard deviation of ~ 0.33 dex, comparable with the dispersion in the luminosity-radius relations. Even considering only the common sample, the probability of non-correlation for C IV and $H\beta$ data is < 0.1 and ~ 60 per cent respectively. The mean value of f for C IV data amounts to 2.40 ± 0.16 . This value is 1.75 times larger than the value obtained by Labita et al. (2006) on the same data, since they adopted a different $R_{\text{BLR}} - \lambda L_{\lambda}$ relation (Pian Falomo & Treves 2005), which provided an estimate of the $H\beta$ broad-line radius rather than the C IV one. The f dependence on FWHM is observed also in C IV data (see figures 5 and 6). No f value deduced from C IV line is found to be consistent with an isotropic model of the BLR. The f -FWHM plot for C IV-based data is fully consistent with a disc-like BLR, both for RLQs and RQQs. In the average value of f , the C IV line appears farther from the isotropic case than the $H\beta$, both being inconsistent with isotropy.

The formally better correlation of imaging-based BH mass estimates with VPs for C IV line rather than for $H\beta$ suggests that the former could be preferable as a mass indicator than $H\beta$, as already proposed by Vestergaard & Peterson (2006) and references therein. If confirmed, this disagrees with recent claims (Baskin & Laor 2005; Sulentic et al. 2007), in which the average blueshift of the high-ionization lines with respect to the rest frame of the host galaxy was interpreted in terms of gas outflow (but see Richards et al. 2002 for a different interpretation). A larger set of quasars with independent estimates of both VPs and M_{BH} , sampling a wider parameter space, is required in order to better address this topic.

6 A SKETCH OF THE BLR DYNAMICS

We discuss how three simple models of the BLR dynamics can account for or contrast with the observed $H\beta$ and C IV line shapes and widths.

Isotropic model:

Up to now, since the geometry of the BLR is poorly understood, an isotropic model has been commonly adopted as a reference. As mentioned in section 5.1, if the BLR is dominated by isotropic motions, with a Maxwellian velocity distribution, the geometrical factor is $f = \sqrt{3}/2$ and the FWHM/ σ_{line} ratio is $\sqrt{8 \ln 2} \approx 2.35$. We find that $H\beta$ FWHM/ σ_{line} ratios are closer to the isotropic case than C IV ones. All the geometrical factors derived from C IV and most of those from $H\beta$ exceed unity, in disagreement with the expected value for this model. Moreover, the isotropic model does not explain the observed f -FWHM relation.

Geometrically thin disc model:

If a disc model is adopted, f depends on 3 free parameters, namely ϑ , c_1 and c_2 in equation 4. Here we assume that the disc is geometrically thin, that is, c_2 tends to zero, c_1 tends to 1 and $f \approx (2 \sin \vartheta)^{-1}$. In the light of the unified scheme of AGNs (Antonucci & Miller 1985), ϑ is supposed to vary between ϑ_{\min} , fixed by the presence of a jet (if any) and ϑ_{\max} , given by the angular dimension of the obscuring torus. Even if these angles are poorly constrained, reasonable values are $0^\circ < \vartheta_{\min} < 10^\circ$ and $30^\circ < \vartheta_{\max} < 55^\circ$ for Type-1 AGNs (see for example the statistical approach in Labita et al. 2006 and in Decarli et al. 2008). Since the line profile depends on the (unknown) radial distribution of the emitting clouds, this model does not constrain the FWHM/ σ_{line} ratio. The thin disc model is able to explain the f values derived from C IV, with ϑ ranging between 5 and 30 degrees. The f -FWHM relation given in figure 5 is accounted for by different inclination angles. On the other hand, H β data are suggestive of a wider range of ϑ values, up to 90° in the thin disc picture. This mismatches with the Type-1 AGN model. Furthermore, objects with both UV and optical spectra exhibit different f values, for C IV and H β lines. Since f depends only on ϑ , different inclination angles for the orbits of the clouds emitting the two lines are needed.

Geometrically thick disc model:

In the case of a thick disc model c_2 is non-negligible. Since H β is emitted in a larger region than C IV, the disc is thinner in the inner region (where C IV line is emitted), and thicker outside (see the *flared disc* model in Collin et al. 2006, and the references therein). This model accounts for the differences in the f factor of the two lines, and the non-correlation of the FWHMs of H β and C IV (figure 7). When the disc is seen almost face-on, the velocity component perpendicular to the disc plane would be larger than the projected rotational component, thus leading to FWHM values larger for H β than for C IV. This picture also explains why H β FWHM/ σ_{line} ratios are close to the expected values for a thermal energy distribution at a given radius from the black hole.

ACKNOWLEDGMENTS

We thank Bradley M. Peterson, Tommaso Treu and the anonymous referee for useful discussions and suggestions. This work is based on observations collected at Asiago observatory. This research has made use of the *VizieR Service*, available at <http://vizier.u-strasbg.fr/viz-bin/VizieR> and of the NASA/IPAC Extragalactic Database (NED) which is operated by the Jet Propulsion Laboratory, California Institute of Technology, under contract with the National Aeronautics and Space Administration. Observed spectra and H β fits are available at www.dfm.uninsubria.it/astro/caqos/index.html.

REFERENCES

- Adelman-McCarthy J., et al. 2007, ApJS, 172, 634
 Antonucci R.R.J. & Miller J.S., 1985, ApJ, 297, 621
 Bahcall J.N., Kirhakos S., Saxe D.H. & Schneider D.P., 1997, ApJ, 479, 642
 Baskin A. & Laor A., 2005, MNRAS, 356, 1029
 Bennert N., Canalizo G., Jungwiert B., Stockton A., Schweizer F., Peng C., Lacy M., 2007, arXiv:0710.1504
 Bentz M.C., Denney K.D., Cackett E.M., 2006, ApJ, 651, 775
 Bentz M.C., Denney K.D., Cackett E.M., Dietrich M., Fogel J.K.J., Ghosh H., Horne K.D., Kuehn C., et al., 2007, ApJ, 662, 205
 Bettoni D., Falomo R., Fasano G. & Govoni F., 2003, A&A, 399, 869
 Blandford R.D., McKee C.F., 1982, ApJ, 255, 419
 Boroson T.A., & Green R.F., 1992, ApJS, 80, 109
 Boyce P.J., Disney M.J., Blades J.C., Boksenberg A., Crane P., Deharveng J.M., Macchetto F.D., Mackay C.D., Sparks W.B., 1998, MNRAS, 298, 121
 Bottorff M., Korista K.T., Shlosman I. & Blandford R.D., 1997, ApJ, 479, 200
 Bressan A., Chiosi C., & Fagotto F., 1994, ApJS, 94, 63
 Brotherton M.S., 1996, ApJS, 102, 1
 Collin S., Kawaguchi T., Peterson B.M., Vestergaard M., 2006, A&A, 456, 75
 Decarli R., Dotti M., Fontana M., Haardt F., 2008, accepted for publication in MNRAS Letters (arXiv:0801.4560)
 Dunlop J.S., McLure R.J., Kukula M.J., et al., 2003, MNRAS, 340, 1095
 Ferrarese L. & Merritt D., 2000, ApJ, 539L, 9
 Ferrarese L., 2006, in Series in High Energy Physics, Cosmology and Gravitation, ‘Joint Evolution of Black Holes and Galaxies’, ed. by M. Colpi, V. Gorini, F. Haardt, U. Moschella (New York - London: Taylor & Francis Group), 1
 Floyd D.J.E., Kukula M.J., Dunlop J.S., et al., 2004, MNRAS, 355, 196
 Francis P.J., Whiting M.T., Webster R.L., 2000, PASA, 17, 56
 Gebhardt K., Bender R., Bower G., et al., 2000, ApJ, 539L, 13
 Graham A.W. & Driver S.P., 2007, ApJ, 655, 77
 Graham A.W., 2007, MNRAS, 379, 711
 Hamilton T.S., Casertano S., Turnshek D.A., 2002, ApJ, 576, 61
 Hooper E.J., Impey C.D. & Foltz C.B., 1997, ApJ, 480, L95
 Kaspi S., Smith P.S., Netzer H., Maoz D., Jannuzi B.T., Giveon U., 2000, ApJ, 533, 631
 Kaspi S., Maoz D., Netzer H., Peterson B.M., Vestergaard M., Jannuzi B.T., 2005, ApJ, 629, 61
 Kaspi S., Maoz D., Netzer H., et al., 2007, ApJ, 659, 997
 King A.R., 2005, ApJ, 635, L121
 Kirhakos S., Bahcall J.N., Schneider D.P. & Kristian J., 1999, ApJ, 520, 67
 Kormendy J. & Richstone D., 1995, ARA&A, 33, 581
 Kotilainen J.K., Falomo R., Labita M., Treves A., Uslenghi M., 2007, ApJ, 660, 1039
 Kuehn C.A., Baldwin J.A., Peterson B.M., Korista K.T., 2008, ApJ, 673, 69
 Labita M., Treves A., Falomo R., Uslenghi M., 2006, MNRAS, 373, 551
 Laor A., Barth A.J., Ho L.C., Filippenko A.V., 2006, ApJ,

636, 83
 Lauer T.R., Tremaine S., Richstone D. & Faber S.M., 2007 (astro-ph/0705.4103)
 Magorrian J., Tremaine S., Richstone D., et al., 1998, *AJ*, 115, 2285
 Mannucci F., Basile F., Poggianti B. M. et al., 2001, *MNRAS*, 326, 745
 Marconi A. & Hunt L., 2003, *ApJ*, 589, L21
 Marziani P., Sulentic J.W., Zamanov R., et al., 2003 *ApJS*, 145, 199
 McGill K.L., Woo J.H., Treu T., Malkan M.A., 2007, astro-ph/0710.1839
 McLeod K.K. & Rieke G.H., 1994, *ApJ*, 431, 137
 McLure R.J. & Dunlop J.S., 2001, *MNRAS*, 327, 199
 McLure R.J. & Dunlop J.S., 2002, *MNRAS*, 331, 795
 McLure R.J. & Jarvis M.J., 2002, *MNRAS*, 337, 109
 Metzroth K.G., Onken C.A., Peterson B.M., 2006, *ApJ*, 647, 901
 Onken C.A., Ferrarese L., Merritt D., Peterson B.M., Pogge R.W., Vestergaard M., Wandel A., 2004, *ApJ*, 615, 645
 Pagani C., Falomo R. & Treves A., 2003, *ApJ*, 596, 830
 Peng C.Y., Impey C.D., Rix H.W., et al., 2006, *ApJ*, 649, 616
 Peterson B.M., Ferrarese L., Gilbert K.M., et al., 2004, *ApJ*, 613, 682
 Phillips M.M., 1978, *ApJS*, 38, 187
 Pian E., Falomo R., Treves A., 2005, *MNRAS*, 361, 919
 Richards G.T., Vanden Berk D.E., Reichard T.A., Hall P.B., Schneider D.P., SubbaRao M., Thakar A.R., York D.G., 2002, *AJ*, 124, 1
 Salviander, S., Shields, G.A., Gebhardt, K. & Bonning, E.W., 2007, *ApJ*, 662, 131
 Sbarufatti B., Treves A., Falomo R., Heidt J., Kotilainen J., Scarpa R., 2006, *AJ*, 132, 1
 Schlegel, et al., 1998, *ApJ*, 500, 525
 Sergeev S.G., Doroshenko V.T., Dzyuba S.A., Peterson B.M., Pogge R.W., Pronik V.I., 2007, *ApJ*, 668, 708
 Suganuma M., Yoshii Y., Kobayashi Y., et al., 2006, *ApJ*, 639, 46
 Sulentic J.W., Zwitter T., Marziani P. & Dultzin-Hacyan D., 2000, *ApJ*, 536, L5
 Sulentic J.W., Bachev R., Marziani P., Negrete C.A., Dultzin D., 2007, *ApJ*, 666, 757
 Treu T., Woo J.H., Malkan M.A., & Blandford R.D., 2007, *ApJ*, 667, 117
 Van Der Marel R.P. & Franx M., 1993, *ApJ*, 407, 525
 Veron-Cetty M.P., & Veron P., 2006, *A&A*, 455, 773
 Vestergaard M., Wilkes B.J., Barthel P.D., 2000, *ApJ*, 538L, 103
 Vestergaard M., & Peterson B.M., 2006, *ApJ*, 641, 689
 Wills B.J. & Browne I.W.A., 1986, *ApJ*, 302, 56
 Woo J.H., Treu T., Malkan M.A., & Blandford R.D., 2006, *ApJ*, 645, 900

APPENDIX A:

A1 Fe II subtraction

The reliability of our zero-order correction was checked as follows:

(i) We observed I Zw001 with the grism 7 setup. The $H\beta$ line was modeled and removed with a 2-gaussian fit.

(ii) For each target, we applied the zero order correction for the Fe II contamination, and we fitted the broad emission of $H\beta$ with a 2-gaussian profile. In order to avoid the $H\beta$ narrow component, we excluded the line central region (~ 1.5 times the spectral resolution) in the fitting procedure, when a narrow $H\beta$ component was clearly observed.

(iii) The spectrum of I Zw001 has been convolved to a gaussian mimicking both the intrinsic and instrumental broadening of the Fe II features. The line width was assumed to be the same as the one measured for $H\beta$, consistently with the most of the literature, thus assuming that Fe II and $H\beta$ emitting regions are nearly the same (but see Kuehn et al. 2008).

(iv) The Fe II template was then scaled in flux and wavelength to match the observed features in the 4400–4650 and 5100–5350 Å ranges. The best fit was subtracted to the observed spectrum.

(v) The narrow lines are modeled on the $[O III]_{5007\text{\AA}}$ line, following McGill et al. (2007): the $[O III]_{4959\text{\AA}}$ flux was assumed to be 1/3 of the $[O III]_{5007\text{\AA}}$ line. Narrow $H\beta$ and He II fluxes are left free in the fitting procedure.

(vi) The resulting spectra only present the $H\beta$ broad emission. We applied a 2-gaussian fit to the $H\beta$ broad component, fitting the range 4750 – 4975 Å.

The template-subtracted FWHM and σ_{line} are compared with the one presented in the paper in figure A1, upper panels. As previously reported by McGill et al. (2007), the FWHMs obtained with and without the subtraction of the Fe II template are in very good agreement: the average difference in the two estimates is negligible (~ 0.03 dex), the standard deviation being ~ 11 per cent of the FWHM values, comparable to the estimated error in the fitting procedure. The estimates of σ_{line} are in agreement, too, but the dispersion is larger: the average difference is ~ 0.04 dex, and the residual standard deviation is ~ 20 per cent.

A2 The fitting function

Several authors (e.g., McGill et al. 2007) preferred the Gauss-Hermite series (Van Der Marel & Franx 1993) when fitting the profile of broad emission lines. In this technique, the observed profile is fitted with a set of orthonormal polynomials (the Hermite series) multiplied to a Gaussian curve. Van Der Marel & Franx (1993) proved that, in most of the situations of astrophysical interest, the lines are well fitted with a series truncated at the fourth order. In this way, the set of independent parameters provided by the fit has a straightforward interpretation, in particular h_3 and h_4 (the coefficient for the third and fourth order of the Hermite series) are related to the line asymmetry and kurtosis.

In order to check the dependence of our results on the adopted fitting function, we applied the Gauss-Hermite fit (extended to the fourth order of the series) to our data, after the Fe II template subtraction described in appendix A1. The FWHM and σ_{line} values obtained with the two profiles are compared in figure A1, lower panels. The FWHM estimates are in good agreement with those adopted in the paper: the average difference (~ 0.05 dex) is negligible within the purposes of our work, with a residual standard deviation of

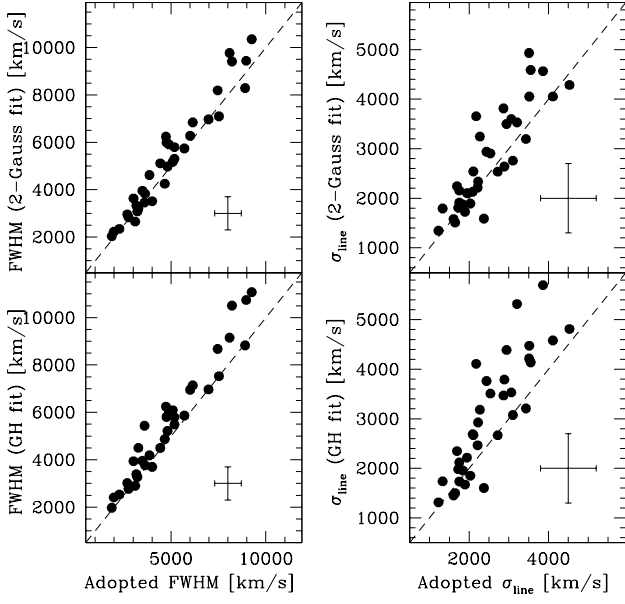


Figure A1. The comparison between various estimates of $H\beta$ FWHM (left) and σ_{line} (right). In the x-axis, the width estimates obtained with our zero-order correction for Fe II emission and the 2-gaussian fit for the broad emission of $H\beta$. In the y-axis, in the upper panel the width estimates obtained with the 2-gaussian technique, after Fe II template subtraction. In the lower panel, the width estimates based on the Gauss-Hermite fit procedure. The dashed lines refer to the 1-to-1 case. Typical error boxes are also shown. All FWHM estimates are consistent. As expected, the σ_{line} values are more sensitive to the correction for Fe II emission and to the fitted function.

~ 13 per cent. A systematic deviation of σ_{line} estimates is observed when comparing the two fitting technique, but the overall average difference (~ 0.08 dex) cannot account for the differences in the $\text{FWHM}/\sigma_{\text{line}}$ ratio observed for C IV and $H\beta$.

